Karbala International Journal of Modern Science

Volume 6 | Issue 1 Article 13

Numerical analysis of three-dimensional MHD flow of Casson nanofluid past an exponentially stretching sheet

Madhusudan Senapati
S 'O' A Deemed to be University, 1madhusudansenapati@gmail.com

Kharabela Swain
Gandhi Institute For Technology, kharabela1983@gmail.com

Sampad Kumar Parida
S 'O' A Deemed to be University, sampadaparida@soa.ac.in

Recommended Citation
Senapati, Madhusudan; Swain, Kharabela; and Parida, Sampad Kumar (2020) "Numerical analysis of three-dimensional MHD flow of Casson nanofluid past an exponentially stretching sheet," *Karbala International Journal of Modern Science*: Vol. 6 : Iss. 1 , Article 13.
Available at: https://doi.org/10.33640/2405-609X.1462

Numerical analysis of three-dimensional MHD flow of Casson nanofluid past an exponentially stretching sheet

Abstract

The convective three dimensional electrically conducting Casson nanofluid flow over an exponentially stretching sheet embedded in a saturated porous medium and subjected to thermal as well as solutal slip in the presence of externally applied transverse magnetic field (force-at-a-distance) is studied. The heat transfer phenomenon includes the viscous dissipation, Joulian dissipation, thermal radiation, contribution of nanofluidity and temperature dependent volumetric heat source. The study of mass diffusion in the presence of chemically reactive species enriches the analysis. The numerical solutions of coupled nonlinear governing equations bring some earlier reported results as particular cases providing a testimony of validation of the present study. The important findings are reported as Casson fluid contributes to accelerate the processes of momentum diffusivity but decelerates the thermal diffusivity. The effects of respective Biot numbers in temperature and concentration distributions are significant whereas cross effects are not. Further, the existence of chemical reaction stabilizes the characteristics of rate coefficients at the surface.

Keywords

Casson fluid, viscous dissipation, Joule heating, radiation, chemical reaction

1. Introduction

The stretching sheet phenomena have a bearing on extrusion of a polymer in a melt spinning processes. In particular, the extrudate from the die is generally drawn and simultaneously stretched into a sheet. Further, the spinning of fibres and glass blowing etc. are some more applications pertaining to this area. Choi [1] developed the concept of nanofluid to enhance the thermal conductivity property of the base fluid.

Nomenclature

x, y, z	Cartesian coordinates (m)
u, v, w	velocity components in x, y and z directions respectively (m/s)
B_0	magnetic field strength (N/mA)
T	temperature of the fluid (K)
C	concentration of the solute (kg/m^3)
T_∞	ambient temperature (K)
C_∞	ambient concentration (kg/m^3)
T_f	reference temperature (K)
C_f	reference concentration (kg/m^3)
q_r	radiative heat flux (W/m)
S^*	heat source coefficient
h_f	convective heat transfer coefficient
h_m	convective mass transfer coefficient
Ec_x, Ec_y	Eckert number
$Kc*$	reaction rate of the solute
Kc	chemical reaction parameter
M	magnetic parameter
Kp	porosity parameter
R	Radiation parameter
D_T	thermophoretic diffusion coefficient (m2/s)
k_f	thermal conductivity of the fluid (m 2/s)
D_B	Brownian motion coefficient (m2/s)
Sc	Schmidt number
Bi_t	thermal Biot number
Bi_c	solutal Biot number
Pr	Prandtl number
S	heat source/sink parameter

Greek symbols

η	similarity variable
$\boldsymbol{\Psi}$	stream function
θ	dimensionless temperature
ϕ	dimensionless concentration
β	Casson fluid parameter
δ	velocity ratio parameter
ρ_f	density of the fluid (kg/m3)
υ_f	kinematic viscosity of the fluid (m 2/s)
μ_f	dynamic viscosity of the fluid (kg/m s)
σ^*	Stefan-Boltzman constant

https://doi.org/10.33640/2405-609X.1462

Buongiorno [2] highlighted the contribution of Brownian motion and thermophoresis to augment the thermal conductivity property of the fluid. Crane [3] discussed a similar solution for steady two dimensional flow caused by stretching a sheet with linearly varying velocity. Rashidi et al. [4] have presented the buoyancy effect on MHD flow of nanofluid over a stretching sheet in presence of thermal radiation. Parida and Mishra [5] have studied heat and mass transfer of MHD nanofluid flow on a stretching sheet in presence of chemical reaction. Swain et al. [6] have studied viscoelastic nanofluid flow past a stretching sheet under the influence of chemical reaction. Nayak et al. [7] have studied the viscoelastic fluid over a stretching sheet considering the chemical reaction of the reacting species. Mahanthesh et al. [8] have analysed numerically the flow of nanofluid over a bidirectional nonlinear stretching with heat flux. A numerical solution was carried out by Swain et al. [9] on MHD nanofluid flow past a stretching sheet with higher order chemical reaction. Krupalakshmi et al. [10] have studied an upper-convected Maxwell fluid flow over a convectively heated stretching sheet with nonlinear thermal radiation. Raza et al. [11] have studied multiple slip effects on MHD non-Newtonian nanofluid flow over a nonlinear permeable elongated sheet. Swain et al. [12] have investigated MHD boundary layer flow of Williamson nanofluid in presence of porous medium and non-uniform heat source. Raza et al. [13] have taken nano Williamson fluid over a stretching sheet with slip boundary conditions.

Casson fluid is an ideal fluid model to represent the flow of blood in thin arteries. Further, MHD flow and heat transfer of Casson fluid in a saturated porous medium find wide applications in polymer industry and biological system. Casson fluid acts sort of an elastic solid above a threshold shear stress and small shear strain. Casson fluid possess limiting characteristics (non-Newtonian fluidity) to represent infinite viscosity at zero shear stress ($\beta \to 0$) and Newtonian viscosity at large stress ($\beta \to \infty$) where β acts as Casson parameter. This is the rare property which Casson fluid possesses. Mukhopadhyay [14] studied the flow and heat transfer of Casson fluid over a nonlinearly stretching surface. Three-dimensional flow of Casson fluid past a linearly stretching porous plate has been studied by Nadeem et al. [15]. Mustafa and Khan [16] have considered Casson nanofluid flow past a nonlinearly stretching sheet. Ullah et al. [17] studied the impact of velocity slip on MHD Casson fluid over a nonlinearly stretching sheet in presence of Newtonian heating in a porous medium. The slip flow analysis of Casson fluid has been studied by Poornima et al. [18]. Sulochana et al. [19] carried out the similarity solution of Casson nanofluid over a stretching sheet. Souayeh et al. [20] have analyzed the Casson nanofluid flow considering nonlinear thermal radiation. Mahanthesh et al. [21] have considered the Hall current and exponential heat source on unsteady heat transport of dusty TiO_2-EO nanoliquid with nonlinear radiative heat. Raza [22] studied the slip effects on MHD stagnation point flow of Casson fluid over a convective stretching sheet with thermal radiation. Raza et al. [23] have presented stability analysis of Darcy-Forchheimer flow of Casson type nanofluid over an exponential sheet. Further, the work of Mebarek-Oudina and Bessaih [24] and Mebarek-Oudina [25] on copper-water nanofluid and Titania nanofluids of different base fluids in cylindrical annulus with heat sources enrich the existing literature for interesting outcomes. Raza et al. [26] considered MHD flow of molybdenum disulfide nanofluid in a channel and Hamrelaine et al. [27] have analyzed the flow characteristics of Jeffery Hamel fluid with suction/injection applying Homotopy Analysis Method (HAM).

Recently, Kumar et al. [28] have studied a three-dimensional convective as well as radiative MHD Casson nanofluid flow over an exponentially accelerated stretching sheet. They have accounted for important characteristics of Casson fluid in respect of flow, heat and mass transfer phenomena by applying homotopy analysis method (HAM), leaving aside the energy losses due to viscous dispassion and Julian dispassion in a non-reactive diffusing species. The present study brings to its fold following aspects: the thermal energy losses due to viscous dissipation as well as Joulian dissipation which affect significantly in a convective momentum, thermal and solutal transport phenomena. For the slow flow, i.e. in the absence of convective terms in the governing equations, the contribution may be neglected. Moreover, industrial fluids are conducting in nature and are chemically reactive also. The inclusion of chemical reaction term makes the study more realistic. The inclusion of dissipative terms in the heat equation renders the analysis so complicated that the analytical/semi-analytical methods may not be applicable. Hence, numerical method has been applied to solve the equations.

2. Formulation of the model

A steady, incompressible, laminar three-dimensional boundary layer flow of an electrically conducting Casson nanofluid over an exponentially stretching sheet in a saturated porous medium is considered. The z-axis is taken normal to the plate and plate lies on xy-plane. The plate is stretched along x and y directions exponentially. A transverse magnetic field is applied in the direction perpendicular to the plate (see Fig. 1). The interaction of the conducting fluid with transversely applied magnetic field generates an electromagnetic force which resists the fluid motion. We have restricted our discussion to low magnetic Reynolds number to avoid the effect of induced magnetic field that paves the way for future study. The constitutive equation for an isotropic and incompressible flow of Casson fluid is given by Refs. [29,30].

$$\tau_{ij} = \begin{cases} 2\left(\mu_B + \dfrac{p_y}{\sqrt{2\pi}}\right)e_{ij}, \pi > \pi_c \\ 2\left(\mu_B + \dfrac{p_y}{\sqrt{2\pi_c}}\right)e_{ij}, \pi < \pi_c \end{cases}$$

where μ_B, p_y are the plastic dynamic viscosity, yield stress of the fluid respectively, $\pi = e_{ij}e_{ij}$, e_{ij} is the $(i,j)^{th}$ component of the deformation rate and π_c is the critical value of π, based on non-Newtonian model. In the present problem, the surviving stress component is τ_{xz}. Now $\tau_{xz} = \mu_B\left(1+\frac{1}{\beta}\right)\left(\frac{\partial w}{\partial x}+\frac{\partial u}{\partial z}\right)$ and $\frac{\partial w}{\partial x} = 0$ where $\beta = \mu_B\frac{\sqrt{2\pi_c}}{p_y}$ is Casson fluid parameter.

Under the above assumption, the governing equations following Kumar et al. [28] are

$$\frac{\partial u}{\partial x}+\frac{\partial v}{\partial y}+\frac{\partial w}{\partial z}=0, \tag{1}$$

$$u\frac{\partial u}{\partial x}+v\frac{\partial u}{\partial y}+w\frac{\partial u}{\partial z}=\upsilon_f\left(1+\frac{1}{\beta}\right)\frac{\partial^2 u}{\partial z^2}-\frac{\sigma B_0^2 u}{\rho_f}-\frac{\upsilon_f u}{K_p^*}, \tag{2}$$

$$u\frac{\partial v}{\partial x}+v\frac{\partial v}{\partial y}+w\frac{\partial v}{\partial z}=\upsilon_f\left(1+\frac{1}{\beta}\right)\frac{\partial^2 v}{\partial z^2}-\frac{\sigma B_0^2 v}{\rho_f}-\frac{\upsilon_f v}{K_p^*}, \tag{3}$$

$$u\frac{\partial T}{\partial x}+v\frac{\partial T}{\partial y}+w\frac{\partial T}{\partial z}=\frac{k_f}{(\rho c)_f}\frac{\partial^2 T}{\partial z^2}+\frac{(\rho c)_p}{(\rho c)_f}\left[D_B\frac{\partial C}{\partial z}\frac{\partial T}{\partial z}+\frac{D_T}{T_\infty}\left(\frac{\partial T}{\partial z}\right)^2\right]-\frac{1}{(\rho c)_f}\left(\frac{\partial q_r}{\partial z}\right)+\frac{\sigma B_0^2}{(\rho c)_f}(u^2+v^2)+\frac{\mu_f}{(\rho c)_f}\left(1+\frac{1}{\beta}\right)\left\{\left(\frac{\partial u}{\partial z}\right)^2+\left(\frac{\partial v}{\partial z}\right)^2\right\}+\frac{S^*}{(\rho c)_f}(T-T_\infty), \tag{4}$$

$$u\frac{\partial C}{\partial x}+v\frac{\partial C}{\partial y}+w\frac{\partial C}{\partial z}=D_B\frac{\partial^2 C}{\partial z^2}+\frac{D_T}{T_\infty}\frac{\partial^2 C}{\partial z^2}-K_c^*(C-C_\infty). \tag{5}$$

The corresponding boundary conditions are given by

$$u=U_w=U_0e^{\frac{x+y}{L}}, v=V_0e^{\frac{x+y}{L}}, w=0, -k_s\left(\frac{\partial T}{\partial z}\right)=h_f\left(T_f-T\right),$$
$$-D_m\left(\frac{\partial C}{\partial z}\right)=h_m\left(C_f-C\right) \text{ at } z=0,$$
$$u\to 0, v\to 0, T\to T_\infty, C\to C_\infty \text{ at } z\to\infty. \tag{6}$$

Following Rosseland approximation the radiative heat flux q_r is formulated as

$$q_r=-\frac{4\sigma^*}{3k^*}\frac{\partial T^4}{\partial y}\Rightarrow\frac{\partial q_r}{\partial z}=\frac{16\sigma^* T_\infty^3}{3(\rho c)_f k^*}\frac{\partial^2 T}{\partial z^2},$$

where σ^* Stefan−Boltzmann constant, k^* is the mean absorption coefficient.

We introduce the following similarity transformations

$$u=U_0e^{\frac{x+y}{L}}f', v=U_0e^{\frac{x+y}{L}}g',$$
$$w=-\sqrt{\frac{\upsilon_f U_0}{2L}}e^{\frac{x+y}{2L}}[f(\eta)+\eta f'(\eta)+g(\eta)+\eta g'(\eta)],$$
$$\eta=z\sqrt{\frac{U_0}{2\upsilon_f L}}e^{\frac{x+y}{2L}}, \theta=\frac{T-T_\infty}{T_f-T_\infty}, \phi=\frac{C-C_\infty}{C_f-C_\infty}.$$

The equations (1)−(5) reduce to

$$\left(1+\frac{1}{\beta}\right)f''' + (f+g)f'' - 2(f'+g')f' - (M+Kp)f' = 0, \tag{7}$$

$$\left(1+\frac{1}{\beta}\right)g''' + (f+g)g'' - 2(f'+g')g' - (M+Kp)g' = 0, \tag{8}$$

$$\left(1+\frac{4}{3}R\right)\theta''+\Pr\begin{bmatrix}(f+g)\theta'+Nb\theta'\phi'+Nt\theta'^2+Ec_x f''^2\\+Ec_y g''^2+MEc_x f'^2+MEc_y g'^2+S\theta\end{bmatrix}=0, \tag{9}$$

$$\phi''+Sc(f+g)\phi'+\frac{Nt}{Nb}\theta''-KcSc\phi=0. \tag{10}$$

The transformed boundary conditions are given by

$$f(0)=0, g(0)=0, f'(0)=1, g'(0)=\delta,$$
$$\theta'(0)=-Bi_t[1-\theta(0)], \phi'(0)=-Bi_c[1-\phi(0)], \quad (11)$$
$$f'(\infty)\to 0, g'(\infty)\to 0, \theta(\infty)\to 0, \phi(\infty)\to 0.$$

where $M=\frac{2\sigma B_0^2 L}{\rho_f U_w}, Kp=\frac{2\upsilon_f L}{U_w Kp^*}, \delta=\frac{V_0}{U_0}, R=\frac{4\sigma^* T_\infty^3}{kk^*}, \Pr=\frac{\upsilon_f}{\alpha_f}, S=\frac{2S^* L}{U_w(\rho c)_f},$

$$Sc=\frac{\upsilon_f}{D_B}, Nb=\frac{(\rho c)_p D_B (C_f-C_\infty)}{(\rho c)_f \upsilon_f}, Nt=\frac{(\rho c)_p D_T (T_f-T_\infty)}{(\rho c)_f T_\infty \upsilon_f},$$

$$Bi_t=\frac{h_f}{k_s}\sqrt{\frac{2\upsilon_f L}{U_w}},$$

$$Bi_c=\frac{h_m}{D_m}\sqrt{\frac{2\upsilon_f L}{U_w}}, Ec_x=\frac{U_w^2}{c_p(T_f-T_\infty)}, Ec_y=\frac{V_w^2}{c_p(T_f-T_\infty)}.$$

The shearing stresses, surface heat and mass fluxes are given by

$$\tau_{wx}=\mu_f\left(1+\frac{1}{\beta}\right)\left(\frac{\partial u}{\partial z}+\frac{\partial w}{\partial x}\right)_{z=0},$$
$$\tau_{wy}=\mu_f\left(1+\frac{1}{\beta}\right)\left(\frac{\partial v}{\partial z}+\frac{\partial w}{\partial y}\right)_{z=0},$$
$$q_w=-k_f\left(\frac{\partial T}{\partial z}\right)_{z=0}+(q_r)_{z=0}, q_m=-D_B\left(\frac{\partial C}{\partial z}\right)_{z=0}.$$

The physical quantities of interest are the skin friction coefficients $C_{fx}=\frac{2\tau_{wx}}{\rho_f U_w^2}, C_{fy}=\frac{2\tau_{wy}}{\rho_f U_w^2}$, Nusselt number $Nu_x=\frac{xq_w}{k_f(T_f-T_\infty)}$, and Sherwood number $Sh_x=\frac{xq_m}{D_B(C_f-C_\infty)}$ are given by

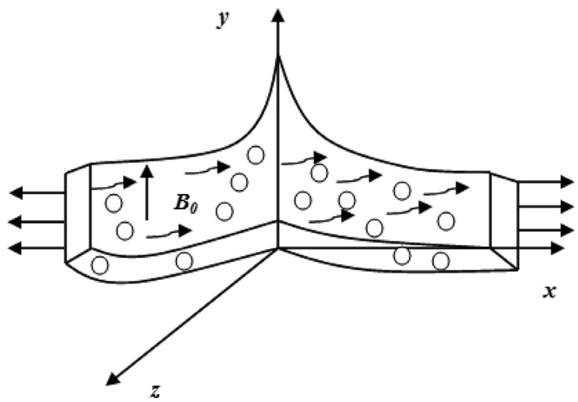

Fig. 1. Flow geometry.

$$\sqrt{\frac{\mathrm{Re}_x}{2}}C_{fx}=\left(1+\frac{1}{\beta}\right)f''(0), \sqrt{\frac{\mathrm{Re}_x}{2}}C_{fy}=\left(1+\frac{1}{\beta}\right)g''(0),$$
$$\left(\frac{\mathrm{Re}_x}{2}\right)^{-1/2}\frac{L}{x}Nu_x=-\left(1+\frac{4}{3}R\right)\theta'(0),$$

and $\left(\frac{\mathrm{Re}_x}{2}\right)^{-1/2}\frac{L}{x}Sh_x=-\phi'(0)$ respectively and $\mathrm{Re}_x=\frac{U_w L}{\upsilon_f}$ (Reynolds number).

3. Numerical method

The coupled, non-linear differential equations (7)−(11) are solved using Runge-Kutta fourth order method in conjuction with shooting technique having accuracy 10^{-5}. In this method, the governing equations are reduced to a set of following first order differential equations.

$$f_1'=f_2,$$
$$f_2'=f_3,$$
$$f_3'=-\left(\frac{\beta}{1+\beta}\right)[(f_1+g_1)f_3-2(f_2+g_2)f_2-(M+Kp)f_2],$$

$$g_1'=g_2,$$
$$g_2'=g_3,$$
$$g_3'=-\left(\frac{\beta}{1+\beta}\right)[(f_1+g_1)g_3-2(f_2+g_2)g_2 -(M+Kp)g_2],$$
$$\theta_1'=\theta_2,$$
$$\theta_2'=-\left(\frac{3\Pr}{3+4R}\right)\times\left[\begin{array}{l}(f_1+g_1)\theta_2+Nb\theta_2\phi_2+Nt\theta_2^2+Ec_x f_3^2\\ +Ec_y g_3^2+MEc_x f_2^2+MEc_y g_2^2+S\theta_1\end{array}\right],$$
$$\phi_1'=\phi_2,$$
$$\phi_2'=-\left[Sc(f_1+g_1)\phi_2-\frac{Nb}{Nt}\left(\frac{3\Pr}{3+4R}\right)\times\left[\begin{array}{l}(f_1+g_1)\theta_2+Nb\theta_2\phi_2+Nt\theta_2^2+Ec_x f_3^2\\ +Ec_y g_3^2+MEc_x f_2^2+MEc_y g_2^2+S\theta_1\end{array}\right]-KcSc\phi_1\right],$$

subject to the initial conditions

$$f_1(0)=0, g_1(0)=0, f_2(0)=1, g_2(0)=\delta,$$
$$\theta_1(0)=\frac{Bi_t+\theta_2}{Bi_t}, \phi_1(0)=\frac{Bi_c+\phi_2}{Bi_c},$$
$$f_3(0)=r_1, g_3(0)=r_2, \theta_2(0)=r_3, \phi_2(0)=r_4,$$

where $r_1, r_2, r_3,$ and r_4 are guess values to be prescribed during computation. A self corrective procedure with the help of Newton−Raphson method has been applied to correct the prescribed guess values to start the process of forward integration.

4. Results and discussion

The following discussion brings out the flow characteristics of Newtonian as well as Casson fluid. The validation has been carried out by comparing the present work with that of Nadeem et al. [15] and Sulochana et al. [31] as particular cases without heat source, thermal dissipation and chemical reaction (Table 1). We have fixed the non-dimensional parameters as $\Pr = Sc = 2$, $M = 0.5, Kp = R = S = \delta = Kc = Ec_x = Ec_y = 0.1$, $Nb = Nt = Bi_t = Bi_c = 0.2$, for the rest part of the discussion and hence omitted in the corresponding graphs.

Table 1
Comparison of the values of $\left(1+\frac{1}{\beta}\right)f''(0)$ for $M = \beta = \delta = 0.5$, $S = Ec_x = Ec_y = Kc = 0$.

M	Kp	β	Nadeem et al. [15]	Sulochana et al. [31]	Present study
0	0	∞	1.0932	1.093252	1.093258
0	0	5	1.1974	1.197425	1.197431
0	0.5	1	1.8361	1.836082	1.836097
10	0	∞	3.3420	3.342020	3.342184
10	0	5	3.6610	3.660730	3.660776
10	0.5	1	4.8310	4.830596	4.830641

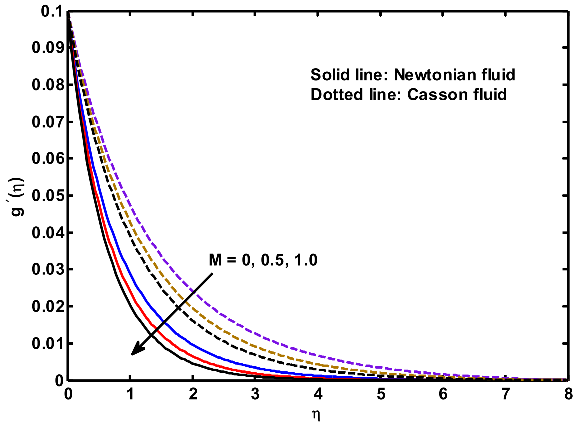

Fig. 3. Influence of M on $g'(\eta)$.

Figs. 2 and 3 present an inverted boundary layer structure. The reason for this phenomenon is attributed to the fact that the stretching velocity of the surface of the sheet $(f'(0)=1)$ exceeds the external stream $(f'(\infty)=0)$. Further, it is observed that the primary velocity of Casson nanofluid exceeds the velocity of Newtonian fluid at all points. It is also seen that at a fixed point, the velocity decreases with increasing magnetic parameter due to a resistive electromagnetic force generated due to interaction of transverse magnetic field with moving conducting fluid. From the graphical representation, it is further revealed that momentum transport gets accelerated in case of Casson fluid as compared to Newtonian fluid. Therefore, Casson fluid contributes to accelerate the processes of momentum diffusivity (Figs. 2−5) but decelerates the thermal diffusivity (Figs. 6−14) evading the effects of other parameters such as $\Pr, R, S, Nb, Nt, Ec_x$, Ec_y, Bi_t and Bi_c. Thus, the decrease in thermal diffusivity sets in a cooling effect during the process of decelerated

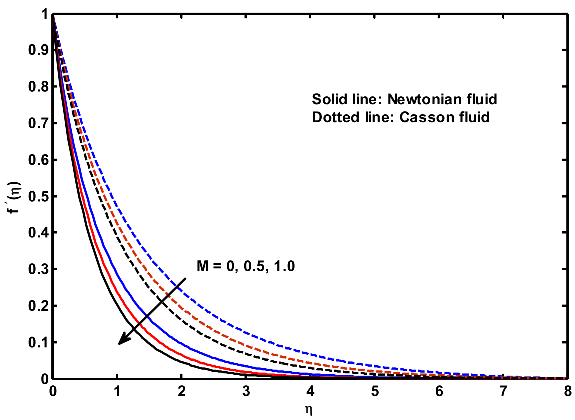

Fig. 2. Influence of M on $f'(\eta)$.

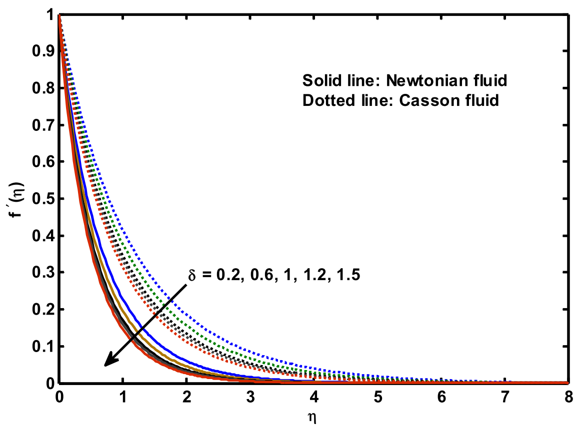

Fig. 4. Influence of δ on $f'(\eta)$.

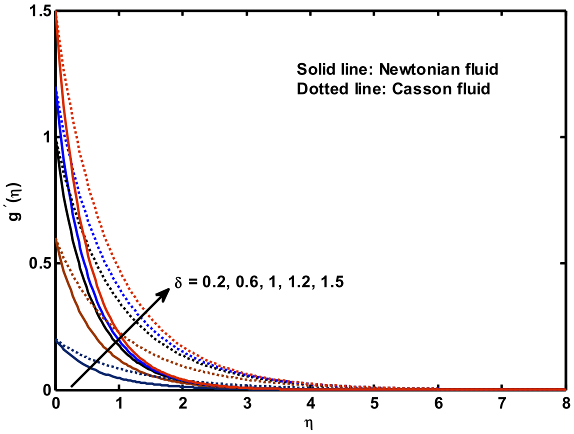

Fig. 5. Influence of δ on $g'(\eta)$.

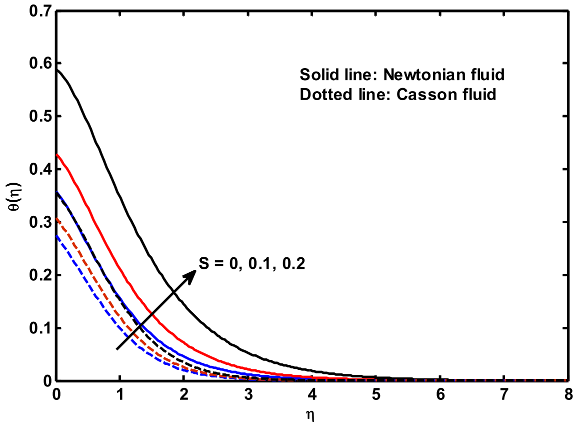

Fig. 8. Influence of S on $\theta(\eta)$.

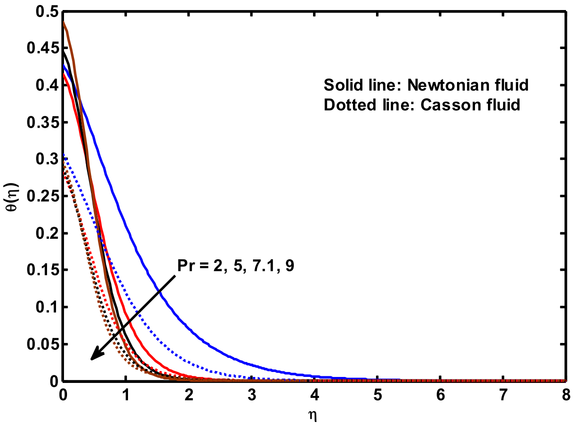

Fig. 6. Influence of Pr on $\theta(\eta)$.

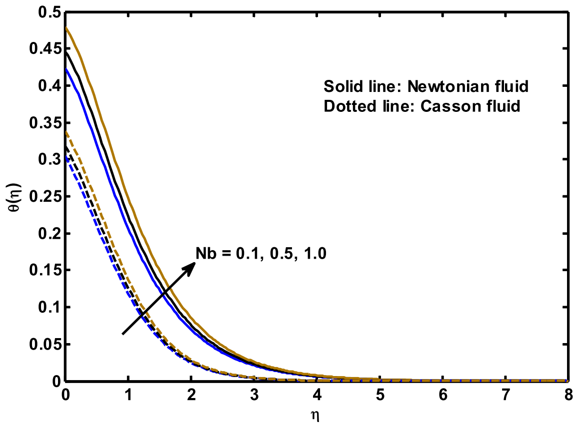

Fig. 9. Influence of Nb on $\theta(\eta)$.

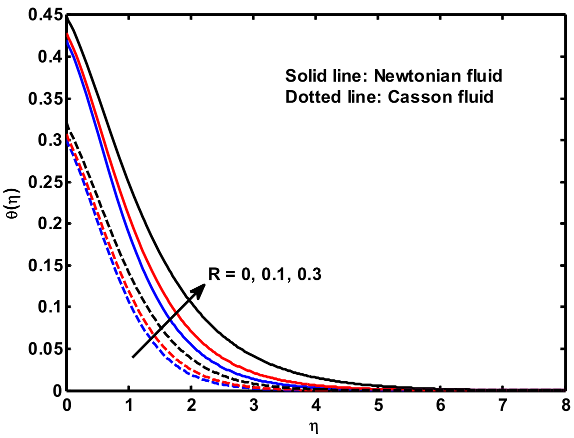

Fig. 7. Influence of R on $\theta(\eta)$.

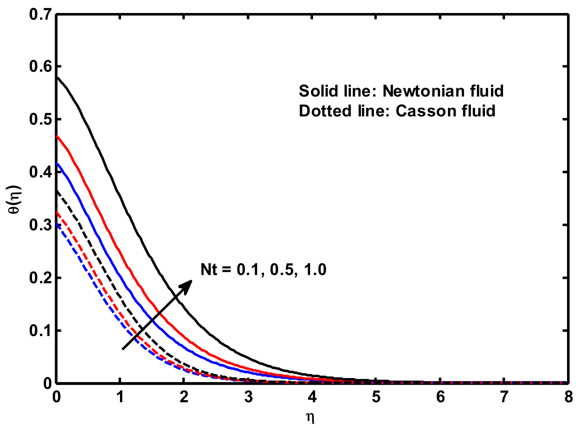

Fig. 10. Influence of Nt on $\theta(\eta)$.

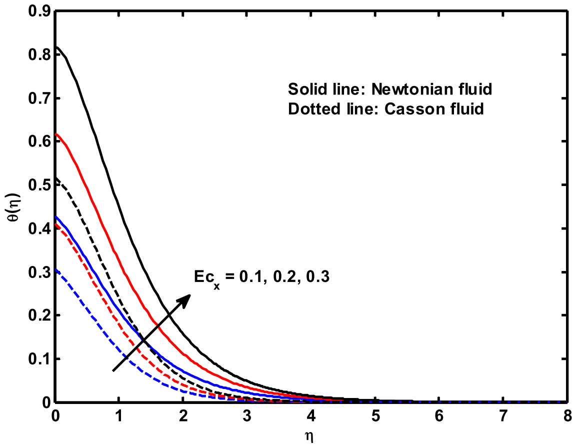

Fig. 11. Influence of Ec_xon $\theta(\eta)$.

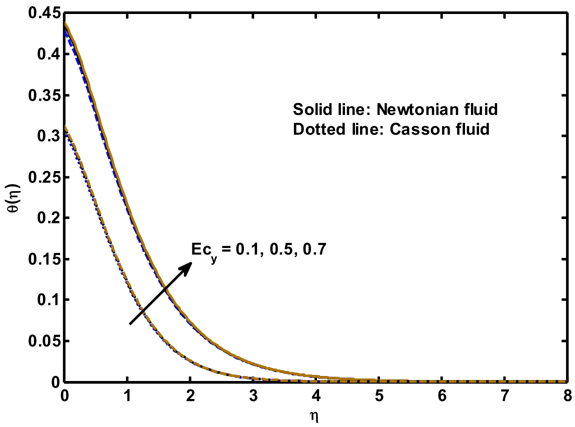

Fig. 12. Influence of Ec_y on $\theta(\eta)$.

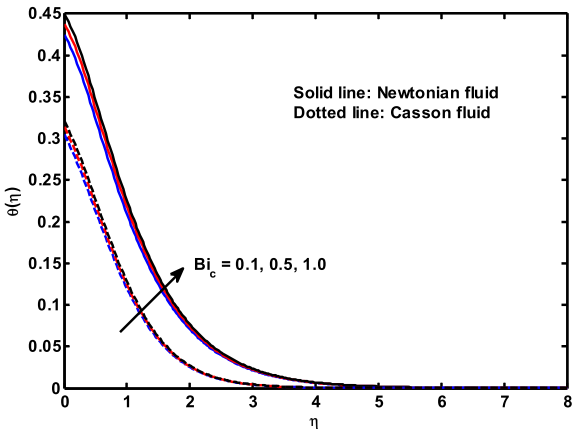

Fig. 13. Influence of Bi_c on $\theta(\eta)$.

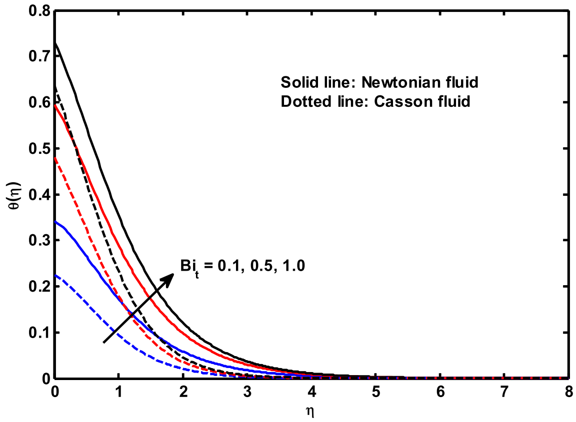

Fig. 14. Influence of Bi_t on $\theta(\eta)$.

momentum diffusivity in the entire flow domain, is a note worthy property of the Casson fluid. This may be attributed to the thermal stratification. Further, it is observed that primary velocity component $f'(\eta)$ of the Casson fluid decreases irrespective of $\delta < 1$ or $\delta \geq 1$ (Fig. 4). In case of secondary velocity $g'(\eta)$, the reverse effect is observed (Fig. 5). This also meets the design requirement whenever necessity arises to accelerate the velocity components of the fluid without raising the temperature of the fluid but changing the velocity ratio (δ).

The effect of higher values of the parameters such as R, S, Nb, Nt, Ec_x, Ec_y , Bi_c and Bi_t is to increase the temperature distribution except the Prandtl number, Pr which reduces the temperature due to low conductivity in the whole of the flow domain (Figs. 6–14). Hence, it may be concluded that other parameters involved posses higher thermal conductivity property than Pr. From close analysis of Figs. 11 and 12, it is seen that the dissipative component Ec_x has a distinct effect on temperature distribution but Ec_y has no such. The effects of respective Biot numbers in temperature and concentration distributions are significant (Figs. 14 and 17) whereas cross effects are not. The effect of Biot number is to be correctly noted down because the conductivity of the solid surface is involved in it whereas the Nusselt number the conductivity of the fluid is involved. However, both determine the rate of heat transfer at the bounding surface from solid to fluid and vice versa [32].

Fig. 15 shows the solutal concentration in the presence of diffusing species. It is observed that higher Schmidt number (i.e. the heavier species) lowers down the level of concentration. Moreover, Newtonian fluid possesses slightly higher concentration level than that of Casson fluid. From Fig. 16, it is seen that for

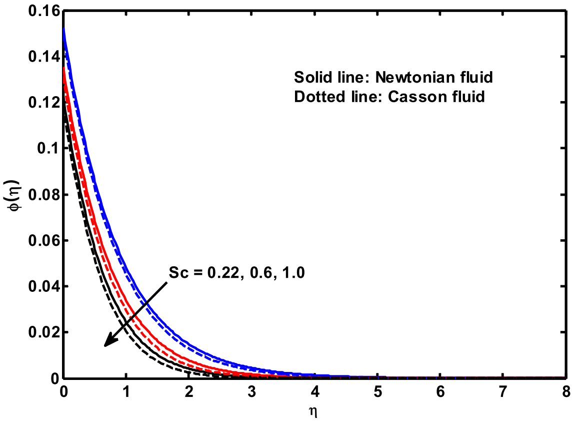

Fig. 15. Influence of Sc on $\phi(\eta)$.

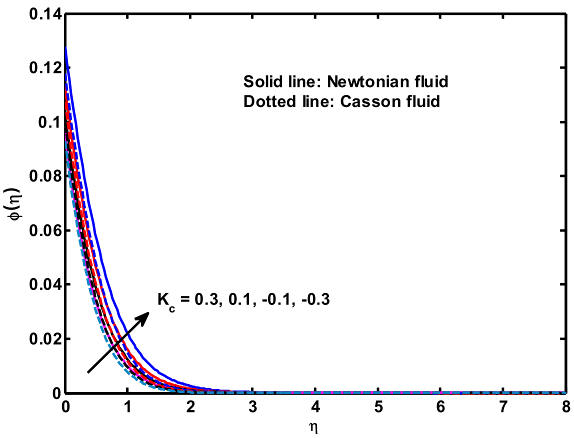

Fig. 16. Influence of Kcon $\phi(\eta)$.

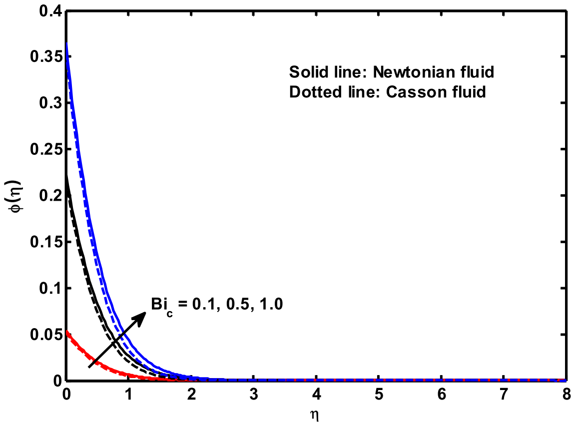

Fig. 17. Influence of Bi_c on $\phi(\eta)$.

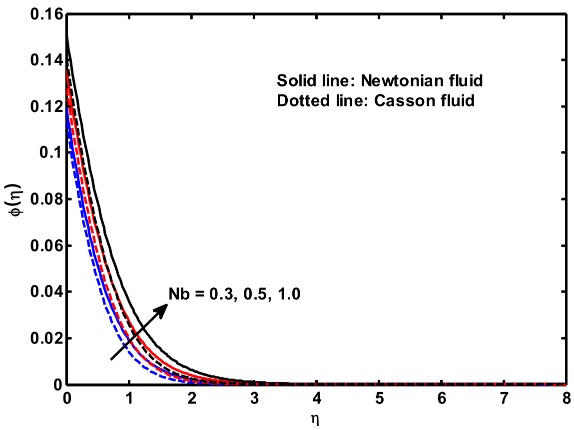

Fig. 18. Influence of Nb on $\phi(\eta)$.

increasing exothermic reaction/constructive reaction $(Kc > 0)$, the solutal concentration decreases due to fast movement of fluid molecules but for $Kc < 0$, in case of endothermic reaction, the opposite effect is observed. On increasing solutal Biot number Bi_c and Nb, the level of concentration increases whereas the level of concentration depletes due to increasing values of Nt (Figs. 17–19).

From the Table 2 it is seen that both the skin friction coefficients bear negative sign and decrease along with the rates of heat and mass transfer. This shows that there exists Reynolds analogy between force co-efficients and surface fluxes [33]. There are two components of wall shear stresses. Both the components decrease as the magnetic parameter (M), velocity ratio

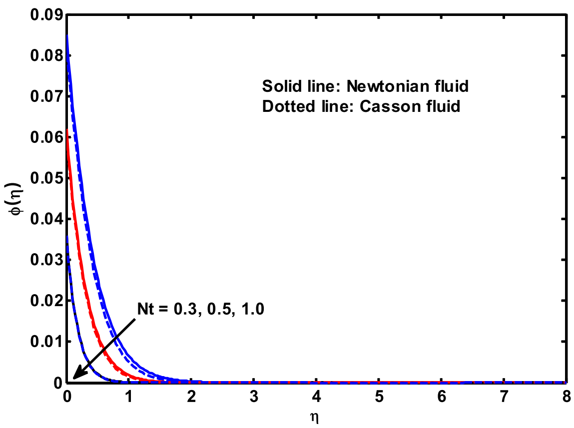

Fig. 19. Influence of Nt on $\phi(\eta)$.

Table 2
Numerical values of $f''(0), g''(0), -\theta'(0)$ and $-\phi'(0)$ when $\beta = Kp = Nb = Nt = 0.5$, $Sc = 0.6$, $\Pr = 5$, $Bi_t = Bi_c = 0.1$.

M	δ	R	Ec_x	Ec_y	S	Kc	$f''(0)$	$g''(0)$	$-\theta'(0)$	$-\phi'(0)$
0	0.1	0	0.1	0.1	0	0	−2.63563	−0.26356	0.08495	−0.15048
0.5	0.1	0	0.1	0.1	0	0	−2.90817	−0.29081	0.07661	−0.23380
1.0	0.1	0	0.1	0.1	0	0	−3.15671	−0.31567	0.06777	−0.32228
1.0	0.5	0	0.1	0.1	0	0	−3.45601	−1.72800	0.06633	−0.36864
1.0	1.0	0	0.1	0.1	0	0	−3.79679	−3.79679	0.05697	−0.43026
1.0	1.0	0.1	0.1	0.1	0	0	−3.79679	−3.79679	0.06774	−0.40227
1.0	1.0	0.5	0.1	0.1	0	0	−3.79679	−3.79679	0.10900	−0.34598
1.0	1.0	0.5	0.3	0.1	0	0	−3.79679	−3.79679	0.04464	−0.73214
1.0	1.0	0.5	0.5	0.1	0	0	−3.79679	−3.79679	−0.06134	−1.36806
1.0	1.0	0.5	0.5	0.3	0	0	−3.79679	−3.79679	−0.34990	−3.09942
1.0	1.0	0.5	0.5	0.5	0	0	−3.79679	−3.79679	−1.04475	−7.26855
1.0	1.0	0.5	0.5	0.5	−0.4	0	−3.79679	−3.79679	−0.08043	−1.48259
1.0	1.0	0.5	0.5	0.5	−0.2	0	−3.79679	−3.79679	−0.18630	−2.11785
1.0	1.0	0.5	0.5	0.5	0.2	0	−2.63150	−3.20519	−0.82438	−5.94496
1.0	1.0	0.5	0.5	0.5	0.4	0	−2.54137	−3.16688	−0.54588	−4.27384
1.0	1.0	0.5	0.5	0.5	0.4	0.1	−2.54137	−3.16688	−0.55785	−4.34570
1.0	1.0	0.5	0.5	0.5	0.4	0.2	−3.78385	−3.78096	−0.71128	−5.26772
1.0	1.0	0.5	0.5	0.5	0.4	−0.1	−2.86427	−3.32147	−0.55795	−4.34664
1.0	1.0	0.5	0.5	0.5	0.4	−0.2	−2.71445	−3.24947	−0.63808	−4.82729

parameter (δ) and the destructive reaction $(Kc > 0)$ increase. Further, it is seen that rate of heat transfer and mass transfer also decrease with an increase in M, δ, $S < 0$ and Kc $(Kc < 0)$. Thus, the decrease in surface flux prevents back flow and thermal instability. Moreover, it is interesting to note that for higher destructive reaction rate coefficient $(Kc > 0)$, both components of shearing stresses increase whereas rate of heat transfer and mass transfer decrease. The effects of R, Ec_x, Ec_y and $S < 0$ (sink) has no effect on shearing stresses but as R increases both the rates of heat and mass transfer increase whereas Ec_x and Ec_y decrease the rate coefficients.

5. Conclusion

Some key findings in the present study are as follows:

- For formation of boundary layer structure, the free stream velocity is to exceed the velocity of the bounding surface.
- Casson fluid contributes to accelerate the processes of momentum diffusivity but decelerates the thermal diffusivity.
- The effect of ratio of characteristic velocities (δ) has an accelerating effect on secondary velocity but decelerating effect on the primary component.
- Eckert number reduces the rate of heat and mass transfer but the thermal radiation favours the same at the bounding surface.
- Casson fluid flow is sensitive to heat source rather than sink. The force coefficients at the bounding surface increase with the heat source $(S > 0)$ but sink has no significant effect.
- In the presence of chemical reaction, all the rate coefficients such as shearing stresses, Nusselt number and Sherwood number bear the same sign with a decreasing effect in heat and mass transfer but opposite effect is observed in cases of shearing stresses.

References

[1] S.U.S. Choi, Enhancing thermal conductivity of fluids with nanoparticles, ASME Fluids Eng. Div. 231 (1995) 99−105.
[2] J. Boungiorno, Convective transport in nanofluids, J. Heat Transf. 128 (2006) 240−250.
[3] L.J. Crane, Flow past a stretching plate, J. Appl. Math. Phys. 21 (1970) 645−647.
[4] M.M. Rashidi, N. Vishnu Ganesh, A.K. Abdul Hskeem, B. Ganga, Buoyancy effect on MHD flow of nanofluid over a stretching sheet in presence of thermal radiation, J. Mol. Liq. 198 (2014) 234−238.
[5] S.K. Parida, S.R. Mishra, Heat and mass transfer of MHD stretched nanofluids in presence of chemical reaction, J. Nanofluids 8 (2019) 143−149.
[6] K. Swain, S.K. Parida, G.C. Dash, MHD flow of viscoelastic nanofluid over a stretching sheet in a porous medium with heat

source and chemical reaction, Ann. Chem. Mater. Sci. 42 (2018) 7−21.

[7] M.K. Nayak, G.C. Dash, L.P. Singh, Heat and mass transfer effects on MHD viscoelastic fluid over a stretching sheet through porous medium in presence of chemical reaction, Propul. Power Res. 5 (2016) 70−80.

[8] B. Mahanthesh, B.J. Gireesha, R.S. ReddyGorla, F.M. Abbasi, S.A. Shehzad, Numerical solutions for magnetohydrodynamic flow of nanofluid over a bidirectional non-linear stretching surface with prescribed surface heat flux boundary, J. Magn. Magn Mater. 417 (2016) 189−196.

[9] K. Swain, S.K. Parida, G.C. Dash, Higher order chemical reaction on MHD nanofluid flow with slip boundary conditions: a numerical approach, Math. Model. Eng. Probl. 6 (2019) 293−299.

[10] K.L. Krupalakshmi, B.J. Gireesha, B. Mahanthesh, R. S Reddy Gorla, Influence of nonlinear thermal radiation and Magnetic field on upper-convected Maxwell fluid flow due to a convectively heated stretching sheet in the presence of dust particles, Commun. Numer. Anal. 1 (2016) 57−73.

[11] J. Raza, M. Farooq, F. Mebarek-Oudina, B. Mahanthesh, Multiple slip effects on MHD non-Newtonian nanofluid flow over a nonlinear permeable elongated sheet: numerical and statistical analysis, Multidiscip. Model. Mater. Struct. 15 (2019) 913−931.

[12] K. Swain, S.K. Parida, G.C. Dash, Effects of non-uniform heat source/sink and viscous dissipation on MHD boundary layer flow of Williamson nanofluid through porous medium, Defect Diffusion Forum 389 (2018) 110−127.

[13] J. Raza, F. Mebarek-Oudina, B. Mahanthesh, Magnetohydrodynamic flow of nano Williamson fluid generated by stretching plate with multiple slips, Multidiscip. Model. Mater. Struct. 15 (2019) 871−894.

[14] S. Mukhopadhyay, Casson fluid flow and heat transfer over a nonlinearly stretching surface, Chin. Phys. B 22 (2013), 074701.

[15] S. Nadeem, R.U. Haq, N.S. Akbar, Z.H. Khan, MHD three dimensional Casson fluid flow past a porous linearly stretching sheet, Alexandria Eng. J. 52 (2013) 577−582.

[16] M. Mustafa, J.A. Khan, Model for flow of Casson nanofluid past a nonlinearly stretching sheet considering magnetic field effects, AIP Adv. 5 (2015), 077148.

[17] I. Ullah, S. Shafie, I. Khan, Effects of slip condition and Newtonian heating on MHD flow of Casson fluid over a nonlinearly stretching sheet saturated in a porous medium, J. King Saud Univ. Sci. 29 (2016) 250−259.

[18] T. Poornima, P. Sreenivasulu, N.B. Reddy, Slip flow of Casson rheological fluid under variable thermal conductivity with radiation effects, Heat Tran. Res. 44 (2014) 718−737.

[19] C. Sulochana, N. Sandeep, V. Sugunamma, B. Rushi Kumar, Aligned magnetic field and cross-difussion effects of a nanofluid over an exponentially stretching surface in porous medium, Appl. Nanosci. 6 (2016) 737−746.

[20] B. Souayeh, M.G. Reddy, P. Sreenivasulu, T. Poornima, M.R. Gorji, I.M. Alarifi, Comparitive analysis on non-linear radiative heat transfer on MHD Casson nanofluid past a thin needle, J. Mol. Liq. 284 (2019) 163−174.

[21] B. Mahanthesh, N.S. Shashikumar, B.J. Gireesha, I.L. Animasaun, Effectiveness of Hall current and exponential heat source on unsteady heat transport of dusty TiO_2-EO nanoliquid with nonlinear radiative heat, J. Comput. Design Eng. 6 (2019) 551−561.

[22] J. Raza, Thermal radiation and slip effects on magnetohydrodynamic (MHD) stagnation point flow of Casson fluid over a convective stretching sheet, Propul. Power Res. 8 (2019) 138−146.

[23] J. Raza, O. Zurni, I. Khan, L.A. Lund Baloch, M. Bakouri, I. Tlili, Stability analysis of Darcy-Forchheimer flow of casson type nanofluid over an exponential sheet: investigation of critical points, Symmetry 11 (2019) 412−430.

[24] F. Mebarek-Oudina, R. Bessaïh, Numerical simulation of natural convection heat transfer of copper-water nanofluid in a vertical cylindrical annulus with heat sources, Thermophys. Aeromechanics 26 (2019) 325−334.

[25] F. Mebarek-Oudina, Convective heat transfer of Titania nanofluids of different base fluids in cylindrical annulus with discrete heat source, Heat Tran. Asian Res. 48 (2018) 135−147.

[26] J. Raza, F. Mebarek-Oudina, A.J. Chamkha, Magnetohydrodynamic flow of molybdenum disulfide nanofluid in a channel with shape effects, Multidiscip. Model. Mater. Struct. 15 (2019) 737−757.

[27] S. Hamrelaine, F. Mebarek-Oudina, M. Rafik Sari, Analysis of MHD Jeffery Hamel flow with suction/injection by homotopy analysis method, J. Adv. Res. Fluid Mech. Therm. Sci. 58 (2019) 173−186.

[28] P.V. Kumar, S.M. Ibrahim, G. Lorenzini, The study of three dimensional radiative mhd casson nanofluid over an exponential porous stretching sheet with heat source under convective boundary conditions, Int. J. Heat Technol. 36 (2018) 1−10.

[29] S. Palaniammal, K. Saritha, MHD viscous Casson fluid flow in the presence of a temperature gradient dependent heat sink with prescribed heat and mass flux, Front. Heat Mass Tran. (FHMT) 10 (2018).

[30] A. Kamran, S. Hussain, M. Sagheer, N. Akmal, A numerical study of hydrodynamics flow in Casson nanofluid combined with Joule heating and slip boundary conditions, Results Phys. 7 (2017) 3037−3048.

[31] C. Sulochana, G.P. Ashwinkumar, N. Sandeep, Similarity solution of 3D Casson nanofluid flow over a stretching sheet with convective boundary conditions, J. Niger. Math. Soc. 35 (2016) 128−141.

[32] H.D. Baehr, K. Stephan, Heat and Mass Transfer, second ed., Springer-Verlag Berlin Heidelberg, 2006, p. 117.

[33] H. Schlichting, K. Gersten, Boundary Layer Theory, in: eighth ed. (Ed.), Springer-Verlag, Berlin Heidelberg, 2000.